

Robust TOA-based Localization with Inaccurate Anchors for MANET

Xinkai Yu, Yang Zheng, *Member, IEEE*, Min Sheng, *Senior Member, IEEE*, Yan Shi, *Member, IEEE*,
and Jiandong Li, *Fellow, IEEE*

Abstract—Accurate node localization is vital for mobile ad hoc networks (MANETs). Current methods like Time of Arrival (TOA) can estimate node positions using imprecise baseplates and achieve the Cram er-Rao lower bound (CRLB) accuracy. In multi-hop MANETs, some nodes lack direct links to base anchors, depending on neighbor nodes as dynamic anchors for chain localization. However, the dynamic nature of MANETs challenges TOA’s robustness due to the availability and accuracy of base anchors, coupled with ranging errors. To address the issue of cascading positioning error divergence, we first derive the CRLB for any primary node in MANETs as a metric to tackle localization error in cascading scenarios. Second, we propose an advanced two-step TOA method based on CRLB which is able to approximate target node’s CRLB with only local neighbor information. Finally, simulation results confirm the robustness of our algorithm, achieving CRLB-level accuracy for small ranging errors and maintaining precision for larger errors compared to existing TOA methods.

Index Terms—mobile ad hoc network, localization, Cram er-Rao lower bound, dynamic anchor, time-of-arrival

I. INTRODUCTION

GLOBAL Positioning System (GPS) is a high-precision positioning system that relies on satellites in space to achieve comprehensive global coverage. However, to balance the trade-off of accuracy and coverage, GPS positioning is not highly accurate in complex environments, such as tunnel detection scenarios or mountain rescue operations [15], [43]. Furthermore, the uncertainties in GPS localization signals are compounded by the distance between satellites and targets. These uncertainties arise from various unfavorable signal phenomena [45], including multipath effects [10], Non Line-of-Sight (NLOS) connections between devices [11], fluctuations in the propagation speed of radio electromagnetic waves [12], and imperfect synchronization among the system clocks of satellites and targets [13].

In GPS-denied or GPS-degraded environments, a mobile ad hoc network (MANET) that constitutes a small number of base anchors and other mobile nodes can effectively adapt to the specific attributes of these restricted areas [16], [40]. Therefore, the utilization of base anchors to determine the positions of other unlocalized blind nodes has become a focus in the local position system in MANETs.

Xinkai Yu, Yang Zheng, Min Sheng, Yan Shi and Jiandong Li are with the State Key Laboratory of Integrated Service Networks, Xidian University, Xi’an 710071, China (e-mail: xinkaiyu@stu.xidian.edu.cn; yangzheng@xidian.edu.cn; mshengxd@gmail.com; yshi@xidian.edu.cn; jdli@xidian.edu.cn).

Wireless localization techniques can be effectively utilized in MANETs without relying on external network infrastructure. These algorithms are classified into two categories based on their approach to measuring absolute point-to-point distances: range-free and range-based methods [41].

Range-free methods leverage network topology and relative node relationships through multi-hop transmission. Examples include Distance Vector-Hop (DV-Hop) [7], multidimensional scaling map (MDS-MAP) [1], and others. While these methods reduce hardware demands on nodes and minimize network overhead, their positioning accuracy is comparatively lower than that of range-based methods [18]. In contrast, range-based methods rely on measurements of physical properties obtained from neighboring nodes. Techniques such as Time of Arrival (TOA) [19], Time Difference of Arrival (TDOA) [20], Angle of Arrival (AOA) [21], Received Signal Strength Indication (RSSI) [22], and their combinations are employed. Among these, TOA and TDOA, which are time-based measurements, are widely utilized due to their optimal balance between accuracy, stability, ease of hardware implementation, and cost efficiency [14].

TOA methods involve measuring the total flight time of a positioning signal from an emitter to a receiver, demanding complete synchronization among all system devices [23]. Conversely, TDOA methods measure the relative time difference in signal reception between two distinct sensors, eliminating the need to synchronize the target clock with the architecture’s sensor clocks [24]. TOA systems offer enhanced adaptability and accuracy in dynamic environments as they operate independently of baseline information. Additionally, TDOA methods stem from TOA methods, as the time difference can be directly derived from the signal’s flight time [25]. Consequently, we focus our research on the TOA architecture for these compelling reasons in this paper.

In the existing research on TOA position systems, various optimization algorithms have been proposed to tackle the node location problem while minimizing localization uncertainties, such as the Linear Least Square (LLS) method [27], Chan algorithm [28], Genetic Algorithms (GA) [29], Particle Swarm Optimization (PSO) [39], and Sparrow Search Algorithm (SSA) [30]. Many of these studies utilize the Cram er-Rao Lower Bounds (CRLB), which serves as a performance metric, setting a lower limit on the variance of any unbiased estimator [5] to characterize the system uncertainties in node distributions. However, most studies tend to treat the CRLB solely as a theoretical performance benchmark to evaluate algorithms, with few integrating it into anchor selection and

positioning optimization [32], [44]. This is mainly because using the CRLB requires prior knowledge of the target's location, an often unattainable requirement in practical scenarios. However, In MANETs, nodes might simultaneously serve as both target points and anchors, providing convenient conditions for utilizing CRLB.

This paper explores a multi-hop MANET in which network nodes can establish communication either through single-hop or multi-hop connections. When the network node is directly connected to the inaccurate base anchors, the existing TOA localization algorithm can achieve the CRLB accuracy. In [24], [35]–[37], the authors use the semidefinite programming (SDP) method to convert the nonconvex coordinate estimation problem into convex problem. Moreover, the authors employ intelligent search algorithms to solve estimate coordinates in [29], [38], [39], also achieving the CRLB accuracy. In this paper, we employ the PSO algorithm for such node types, using it as a basis for subsequent node estimation.

In MANETs, direct localization via base anchors is often infeasible. This necessitates the identification of "dynamic anchor" neighbor nodes, through which localization is conducted in a cascading fashion. The position information of these anchors is subject to the CRLB for preceding-level node localization. In this paper, we propose an advanced two-step TOA-based localization method using the CRLB. The first step involves using the iterative Chan and PSO method (iChan-PSO) to optimize dynamic anchor positions and update CRLB values. In the second step, we combine node mobility and optimized anchors, utilizing the PSO method to obtain the final result. In this research, these two steps facilitate the selection of dependable neighbor nodes as dynamic anchors where base anchors are unobtainable for direct positioning.

In summary, the major contributions of this paper are listed as follows:

- Given the limited amount of base anchors and potential positional inaccuracies, we derived the CRLB for the estimated coordinate error of any node in a multi-level cascading localization scheme within MANETs.
- Our proposed advanced two-step TOA algorithm effectively leverages local information, including neighbor node's positions and multi-level CRLBs, to address the issue of poor localization accuracy caused by large observed errors.
- We extend the static algorithm by utilizing the continuity of position estimation where nodes exhibit highly dynamic movements in MANETs. The proposed dynamic algorithm aims to enhance the robustness of positioning accuracy in dynamic scenarios.

The remainder of this paper is structured as follows. Section II presents an overview of the localization network model in multi-hop MANETs. In Section III, we derive the CRLB for cascading TOA localization within our network model. Section IV discusses our designed TOA localization method in MANETs. In Section V, we evaluate the performance of our proposed algorithm and compare it with other TOA-based wireless localization methods. Finally, we conclude our paper in Section VI.

Main notations are summarized in Table I.

TABLE I. NOTATION LIST

lowercase x	scalar
bold lowercase \mathbf{x}	vector
bold uppercase \mathbf{X}	matrix
$\hat{x}, \hat{\mathbf{x}}$	estimate of a variable
$\ \mathbf{x}\ $	Euclidean norm of a vector
$\text{tr}(\mathbf{X})$	trace of a matrix
$[\mathbf{X}]_{u:v,m:n}$	sub-matrix with the u^{th} to v^{th} rows and the m^{th} to n^{th} columns
$[\mathbf{X}]_{u,v}$	entry at the u^{th} row and v^{th} column of a matrix
$\mathbb{E}[\cdot]$	expectation operator
$\text{diag}(\cdot)$	diagonal matrix with the elements inside
$\mathbf{s}_i, \tilde{\mathbf{s}}_i$	true coordinates and observed coordinates of the i^{th} base anchor or dynamic anchor
\mathbf{p}^k	the target blind node at level-k
r_i	observed distance between target node \mathbf{p}^k and \mathbf{s}_i
r_{ij}	observed distance between \mathbf{s}_i and \mathbf{s}_j
$D(\cdot), d(\cdot)$	dynamic anchor set and its count
\mathbf{L}_i	set of level-i nodes
\mathbf{n}_{k-1}	total count of nodes from the level k-1 and below
p_q^k, s_{iq}	the q^{th} element of vectors \mathbf{p}^k and \mathbf{s}_i
\mathcal{F}	Fisher information matrix
σ_{ci}^2	CRLB for the i^{th} dynamic anchor
θ	parameter vector
$\sigma_i^2, \delta_i^2 \mathbf{I}_2$	Gaussian variance of distance and base anchors
$B(\mathbf{s}, r)$	circular neighborhood centered at \mathbf{s} with a radius r

II. NETWORK MODEL

In the realm of MANETs, wireless localization systems hold significant importance across various domains such as emergency response, environmental monitoring, and bolstering security measures [2], [15], [40]. Figure 1 illustrates a crucial application in military settings, enabling swift coordination among personnel and equipment during maneuver warfare. All combatants, communication vehicles, unmanned aerial vehicles, and other mobile devices function as network nodes equipped with omnidirectional antennas for signal transmission and reception. By synchronizing the ad hoc nodes, receiving units determine transmission times, enabling distance calculations between nodes based on data signal transmission times.

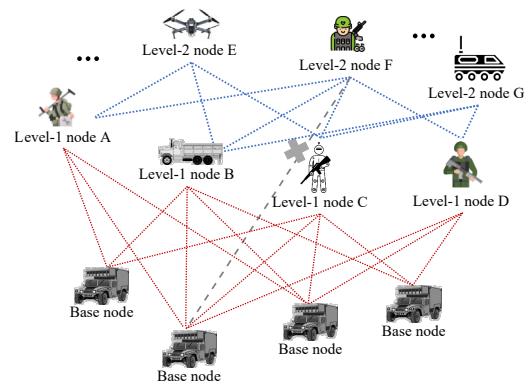


Fig. 1. Localization system scenario based on TOA in MANET

A hierarchical approach is a common strategy for managing and organizing network nodes based on functionality, capabilities, resources, and contributions [6], [42]. This paper employs a hierarchical methodology for node localization, focusing on the transmission radius between each node in the network,

as depicted in Fig. 1. Within this method, four imprecise base anchors, possessing prior positional knowledge, serve as level-0 nodes. Typically, these anchors require manual deployment in locations like rear command centers or control consoles for practical implementation. In TOA localization within an m -dimensional scenario, a minimum of $m+1$ anchor points is necessary for accurate localization. Consequently, level-1 nodes need at least $m+1$ neighboring base anchors, such as A, B, C, and D, enabling direct localization from categorized level-0 base anchors.

Nodes beyond the second level face an insufficient number of neighbor base anchors for direct localization, prompting reliance on lower-level nodes for support. In this context, level-2 nodes utilize level-1 nodes and partial level-0 nodes from single-hop neighbors, serving as "dynamic anchors" to enhance location information within our framework. For instance, node F's dynamic anchor set would comprise {A, B, C, D}.

To generalize, nodes at any level can leverage neighbors from lower levels for localization. Consider a level- k node; it can utilize dynamic anchors from level $k-1$ and below, provided at least one level $k-1$ node acts as a dynamic anchor. To maintain order in localization, it is not allowed for the target point and its dynamic anchor to be at the same level. This approach guarantees each node contributes to the network's position estimation. In practice, node localization typically proceeds from lower to higher levels, with the weakening of connections to base anchors as the level increases.

We are dealing with a network including n_0 level-0 nodes with prior positional information that serve as base anchors. All network nodes, including base anchors, are subject to dynamic positional changes, and the initial position information of base anchors is imprecise. For simplicity, we consider a two-dimensional scenario, it is easy to extend for three-dimensional case. Let $\mathbf{s}_i^0 = (x_i, y_i)^T$ represents the true but unknown coordinates of the i^{th} base anchor. We assume that β_i is a zero-mean white Gaussian vector with known variance $\delta_i^2 \mathbf{I}_2$. The positions of the base anchors can be represented as

$$\tilde{\mathbf{s}}_i^0 = \mathbf{s}_i^0 + \beta_i, \quad i = 1, 2, \dots, n_0. \quad (1)$$

Let $\mathbf{p} = (x, y)^T$ be the coordinates of an unknown target node. Define $d_i = \|\mathbf{p} - \mathbf{s}_i\|$ as the unknown distance between i^{th} available dynamic anchor and the target node. Assuming line-of-sight signal propagation, the asynchronous TOA measurements can be denoted as

$$r_i = d_i + n_i, \quad i = 1, 2, \dots, N. \quad (2)$$

where N represents the number of dynamic anchors for unknown target \mathbf{p} . Here, $n_i \sim \mathcal{N}(0, \sigma_i^2)$ represents the Additive Gaussian White Noise (AWGN) with a variance σ_i^2 . In MANETs, network nodes exhibit the capability to dynamically adjust their behavior, configurations, and connection patterns in response to changing network conditions, thereby catering to varying environments and requirements [33]. For any target node, its available dynamic anchors can be any node other than itself, determined by the network topology and node level. Therefore, the node localization challenge within MANETs can be segmented into two main aspects: the localization of

level-1 nodes, and the localization of nodes at level-2 or higher. How to utilize inaccurate base anchors and dynamic anchors to localize other blind nodes is the focus of our research.

III. CRAMÉR-RAO LOWER BOUND FOR TOA-BASED LOCALIZATION IN MANETS

The CRLB, obtained from the inverse of the Fisher Information Matrix (FIM), represents the minimum achievable error in positioning estimation, independent of the positioning algorithm employed. Numerous studies focus on CRLB in TOA localization errors [5], [34]. However, most derivations only take into account the direct connection between the target source and base anchors. In MANETs, a large number of nodes cannot directly connect to base anchors and instead rely on multi-hop connections for indirect localization. In this section, we provide an exposition on the characterization of the CRLB for nodes at any level under the TOA measurement model and network hierarchy, which serve as both evaluation criteria and guiding principles for designing TOA-based localization in MANETs.

Assume that the observed signal $x(t)$ contains information related to the real parameter θ . For a sample vector, the corresponding estimator $\hat{\theta}$ can be derived from a single sample vector $\mathbf{x} = \{x_1, x_2, \dots, x_n\}^T$. Considering an unbiased estimator, the Cramér-Rao bound theorem establishes a necessary and sufficient condition for it to be an optimal estimator. Treating \mathbf{x} as a random variable, the conditional probability density function $f(\mathbf{x}|\theta)$ can be constructed based on the real parameter θ . The Cramér-Rao bound provides the lower limit for the mean square error (MSE) of the estimator $\hat{\theta}$, which can be given by

$$\sigma_{\hat{\theta}}^2 = \mathbb{E} [(\hat{\theta} - \theta)^2] \geq \frac{1}{J(\theta)} \quad (3)$$

where $J(\theta)$ represents the FIM, and $\sigma_{\hat{\theta}}^2$ signifies the MSE of estimator $\hat{\theta}$. The elements of the FIM are calculated through the second derivative of the logarithm of the likelihood function concerning the parameters, and can be concisely expressed as

$$J(\theta) = -\mathbb{E} \left\{ \frac{\partial^2}{\partial \theta^2} \ln f(\mathbf{x}|\theta) \right\} \quad (4)$$

In the context of TOA-based positioning in MANETs, each node obtains range estimates to its neighbor nodes within the communication range. We consider a MANET includes n_0 base anchors which serve as level-0 nodes and the number of nodes from level 1 to the highest level m is denoted as n_1, n_2, \dots, n_m , respectively. Meanwhile, we designate the set of level- i nodes as \mathbf{L}_i , with a corresponding node count of n_i . Consider the unknown target node at level k , where k is greater than or equal to 1. For target node \mathbf{p}^k , let $D(\mathbf{p}^k)$ be the dynamic anchor set, representing a combination of anchors for localization and can be written as

$$D(\mathbf{p}^k) = \left\{ \mathbf{s}_i \mid \|\mathbf{p}^k - \mathbf{s}_i\| \leq R, \mathbf{s}_i \in \sum_{i=0}^{k-1} \mathbf{L}_i \right\} \quad (5)$$

where $d(\mathbf{p}^k) = |D(\mathbf{p}^k)|$ denotes the number of dynamic anchors, R is the communication radius. For simplicity, we set $d(\mathbf{p}^k) = N$ in the subsequent derivations.

To determine the CRLB under the general TOA measurement model in MANETs, we assume that the measurement noises in (1) and (2) are both independent and identically distributed (i.i.d.). Gaussian random variables of base anchor positions and observed distances with zero mean and variance $\delta^2 \mathbf{I}_2$ and σ^2 . Define $\boldsymbol{\theta} = (\mathbf{p}^k, \mathbf{L}_{k-1}, \mathbf{L}_{k-2}, \dots, \mathbf{L}_0)$ is the estimator in the Maximum Likelihood Estimator (MLE). Under the i.i.d. assumption, the joint conditional probability density function of the observed distance is defined as

$$p(\boldsymbol{\theta}) \triangleq p(r_{ij}, r_i, \tilde{\mathbf{L}}_0 | \mathbf{p}^k, \mathbf{L}_0, \dots, \mathbf{L}_{k-1}) \quad (6)$$

where r_i denotes the observed distance between the target node \mathbf{p}^k and its i^{th} dynamic anchors. Considering the observed errors in the formula (1) and (2), $p(\boldsymbol{\theta})$ can be rewritten as

$$p(\boldsymbol{\theta}) = \prod_{i=1}^N \left[\frac{1}{\sqrt{2\pi\sigma^2}} \exp\left(-\frac{(r_i - \|\mathbf{p}^k - \mathbf{s}_i\|)^2}{2\sigma^2}\right) \right] \times \prod_{i=1}^{\mathbf{n}_{k-1}} \prod_{j=1}^{d(\mathbf{s}_i)} \left[\frac{1}{\sqrt{2\pi\sigma^2}} \exp\left(-\frac{(r_{ij} - \|\mathbf{s}_i - \mathbf{s}_j\|)^2}{2\sigma^2}\right) \right] \times \prod_{i=1}^{\mathbf{n}_0} \left[\frac{1}{\sqrt{2\pi\delta^2}} \exp\left(-\frac{\|\mathbf{s}_i^0 - \tilde{\mathbf{s}}_i^0\|^2}{2\delta^2}\right) \right] \quad (7)$$

where \mathbf{n}_{k-1} represents the total number of network nodes from the level $k-1$ and below. Ignoring the constant term, the log-likelihood function of the location estimation is given by

$$\begin{aligned} \mathbf{L}(\boldsymbol{\theta}) = & -\frac{1}{2\sigma^2} \sum_{i=1}^N (r_i - \|\mathbf{p}^k - \mathbf{s}_i\|)^2 \\ & -\frac{1}{2\sigma^2} \sum_{i=1}^{\mathbf{n}_{k-1}} \sum_{j=1}^{d(\mathbf{s}_i)} (r_{ij} - \|\mathbf{s}_i - \mathbf{s}_j\|)^2 \\ & -\frac{1}{2\delta^2} \sum_{i=1}^{\mathbf{n}_0} \|\mathbf{s}_i^0 - \tilde{\mathbf{s}}_i^0\|^2. \end{aligned} \quad (8)$$

Therefore, the dimensionality of the FIM is $2(\mathbf{n}_{k-1} + 1)$ in the two-dimensional scenario consistent with estimator $\boldsymbol{\theta}$. From (8), we can determine the (m, n) th element in the FIM as

$$[\mathcal{F}]_{m,n} = \sum_{i=1}^N \frac{(p_m^k - s_{im})(p_n^k - s_{in})}{\sigma^2 \|\mathbf{p}^k - \mathbf{s}_i\|^2}, 1 \leq m \leq n \leq 2 \quad (9)$$

Similarly, for $1 \leq m \leq 2 < n \leq 2(\mathbf{n}_{k-1} + 1)$, define $n = 2n_1 + n_2$, we have

$$[\mathcal{F}]_{m,n} = \frac{(p_m^k - s_{n_1 m})(p_n^k - s_{n_1 n_2})}{\sigma^2 \|\mathbf{p}^k - \mathbf{s}_{n_1}\|^2} \quad (10)$$

Additionally, for $3 \leq m \leq n \leq 2(\mathbf{n}_{k-1} + 1)$, define $m = 2m_1 + m_2$ and $n = 2n_1 + n_2$, we have

$$[\mathcal{F}]_{m,n} = \begin{cases} \frac{(s_{m_1 m_2} - s_{n_1 m_2})(s_{m_1 n_2} - s_{n_1 n_2})}{\sigma^2 \|\mathbf{s}_{m_1} - \mathbf{s}_{n_1}\|^2}, & m_1 \neq n_1 \\ \sum_{i=1}^{d(\mathbf{s}_{m_1})} \frac{(s_{m_1 m_2} - s_{im_2})(s_{m_1 n_2} - s_{in_2})}{\sigma^2 \|\mathbf{s}_{m_1} - \mathbf{s}_i\|^2}, & m_1 = n_1 \leq \mathbf{n}_{k-1} - \mathbf{n}_0 \\ \sum_{i=1}^{d(\mathbf{s}_{m_1})} \frac{(s_{m_1 m_2} - s_{im_2})^2}{\sigma^2 \|\mathbf{s}_{m_1} - \mathbf{s}_i\|^2} + \frac{1}{\delta^2}, & \mathbf{n}_{k-1} - \mathbf{n}_0 \leq m_1 \leq \mathbf{n}_{k-1} \\ & , m_1 = n_1, m_2 = n_2 \end{cases} \quad (11)$$

where $m_2, n_2 \in \{1, 2\}$. The detailed derivation of the FIM can be found in the Appendix. Hence, the CRLB of the unbiased estimate \mathbf{p}^k is

$$\sigma_c^2 = \text{tr}\{[\mathcal{F}^{-1}]_{1:1,2:2}\} = \sum_{i=1}^2 [\mathcal{F}^{-1}]_{i,i} \quad (12)$$

IV. ROBUST TOA-BASED LOCALIZATION ALGORITHM FOR MANETS

In this section, we design a TOA-based localization algorithm to make it suitable for dynamic scenarios in MANETs. For level-1 nodes which can directly utilize base anchors for localization, we employ existing algorithms to achieve localization error close to the CRLB level [35]–[37], [39]. For level-2 and higher-level nodes, due to the lack of sufficient directly connected base anchors, we propose an advanced TOA-based positioning algorithm that utilizes dynamic anchors while considering the CRLB. Our designed iCHAN-PSO method achieves the correction of dynamic anchor positions and updates the corresponding CRLB weights. Additionally, our two-step TOA method integrates node mobility to address more complex network scenarios.

A. TOA Localization Algorithm for Level-1 Nodes

For level-1 nodes, their neighbors possess a sufficient number of base anchors for localization. Thus, the level-1 node position problem can be transformed into source localization with anchor position uncertainties, without considering the multi-hop conditions in MANETs. Under the mutually independent Gaussian noise of base anchor positions and observed distance, we can write the MLE of one level-1 node as follows

$$\min_{\mathbf{p}^1, \mathbf{s}_i^0} \sum_{i=1}^{d(\mathbf{p}^1)} \frac{(r_i - \|\mathbf{p}^1 - \mathbf{s}_i^0\|)^2}{\sigma^2} + \sum_{i=1}^{d(\mathbf{p}^1)} \frac{\|\tilde{\mathbf{s}}_i^0 - \mathbf{s}_i^0\|^2}{\delta^2} \quad (13)$$

where \mathbf{p}^1 and \mathbf{s}_i^0 are the optimization parameters of one level-1 target node and the i^{th} base anchors. The above problem is nonlinear and nonconvex, and the MLE is hard to achieve. In this paper, we employ the PSO algorithm to obtain estimates for these level-1 nodes. Similar to source localization with anchor position uncertainties, it can be proven that the level-1 node localization achieves the CRLB accuracy in [39].

B. TOA Localization for Higher-Level MANET Nodes

For positioning nodes at level 2 or above, the simplest approach is to utilize the observed distances between all neighbor nodes in network. Take the positioning of level-2 nodes as an example. To achieve a global solution, the MLE of \mathbf{p}^2 can be constructed as

$$\min_{\mathbf{p}^2, \mathbf{p}_i^1, \mathbf{s}_i^0} \sum_{i=1}^{d(\mathbf{p}^2)} \frac{(r_i - \|\mathbf{p}^2 - \mathbf{s}_i\|)^2}{\sigma^2} + \sum_{i=1}^{\mathbf{n}_0} \frac{\|\tilde{\mathbf{s}}_i^0 - \mathbf{s}_i^0\|^2}{\delta^2} + \sum_{i=1}^{d(\mathbf{p}^1)} \sum_{j=1}^{d(\mathbf{s}_i)} \frac{(r_{ij} - \|\mathbf{s}_i - \mathbf{s}_j\|)^2}{\sigma^2}. \quad (14)$$

If solved appropriately, the global MLE can reach the CRLB because it is consistent with the likelihood function in formula (8). However, there are several issues that prevent its application in MANETs. Firstly, the acquisition of global information inevitably increases network overhead. Additionally, as the node level increases, the complexity and dimension of this global information also increase, leading to increased complexity of the MLE.

In the this subsection, we present the derivation of the proposed two-step TOA method for network nodes at level 2 or above and conclude it in Algorithm 2. Our method solely relies on the estimated positions and distance information of dynamic anchors, along with their CRLBs. These local information can be transmitted through single-hop connections, significantly reducing network overhead and algorithm complexity.

To illustrate our designed algorithm, we take the localization of level- k node \mathbf{p}^k as an example, where $k \geq 2$. The total number of dynamic anchors that can be used for location is N . The i^{th} dynamic anchor coordinates and CRLBs are \mathbf{s}_i and σ_{ci}^2 , respectively. If the i^{th} dynamic anchor is not a base anchor, we can solve the CRLB by formula (12); otherwise $\sigma_{ci}^2 = \delta^2$, when the dynamic anchor is level-0 node. Thus, we can redefine the MLE objective function for \mathbf{p}^k and \mathbf{s}_i based on the CRLBs as follows

$$\min_{\mathbf{p}^k, \mathbf{s}_i} \sum_{i=1}^N \frac{(r_i - \|\mathbf{p}^k - \mathbf{s}_i\|)^2}{\sigma^2} + \sum_{i=1}^N \frac{\|\tilde{\mathbf{s}}_i - \mathbf{s}_i\|^2}{\sigma_{ci}^2}. \quad (15)$$

Considering that intelligent search algorithms offer higher precision in solving likelihood estimation problems compared to traditional mathematical methods, we employ the PSO algorithm to solve this problem. In order to avoid optimization getting trapped in local optima, it is necessary to narrow down the search space. Firstly, considering \mathbf{s}_i as a dynamic anchor with its own position information $\tilde{\mathbf{s}}_i$ after the previous level positioning, and base on it setting the search range. Similarly, for node \mathbf{p}^k itself, we introduce the iterative Chan algorithm to obtain the approximate position to set the initial search range. In comparison to the standard Chan algorithm used for solving the TOA localization equation, our iterative Chan algorithm can handle coordinate estimation when the observed distance errors between nodes remain unknown. We name this method by iterative Chan or iChan for short.

For the objective function in (15), we assume $\tilde{\mathbf{s}}_i = \mathbf{s}_i$ and solely estimate \mathbf{p} to obtain its approximate estimation. During the first iteration process, assume that $\mathbf{e} = (e_1, e_2, \dots, e_N)^T$ is squared error vector between d_i^2 and $\|\mathbf{p} - \mathbf{s}_i\|^2$, where $i = 1, 2, \dots, N$.

$$\mathbf{e} = \begin{bmatrix} d_1^2 - R_1 \\ d_2^2 - R_2 \\ \vdots \\ d_N^2 - R_N \end{bmatrix} - \begin{bmatrix} -2x_1 & -2y_1 & 1 \\ -2x_2 & -2y_2 & 1 \\ \vdots & \vdots & \vdots \\ -2x_N & -2y_N & 1 \end{bmatrix} \begin{bmatrix} x \\ y \\ x^2 + y^2 \end{bmatrix} \quad (16)$$

where $R_i = x_i^2 + y_i^2$. To simplify, we rewritten the squared error vector in (16) as $\mathbf{e} = \mathbf{h} - \mathbf{G}\mathbf{z}_m$.

The standard Chan algorithm assumes that the squared error vector \mathbf{e} follows a Gaussian distribution, which simplifies the

Algorithm 1 Iterative Chan (iChan) Algorithm

Input:

- Dynamic anchors with errors $\tilde{\mathbf{s}}_i, i = 1, 2, \dots, N$;
- Observed distances r_i between \mathbf{s}_i and target \mathbf{p} ;
- Parameters: maximum iteration count $iter$ and convergence threshold ϵ

Output: The estimated target coordinates $\tilde{\mathbf{p}}$;

- 1: Initialize the error vector covariance matrix $\mathbf{Q} = \mathbf{I}_N$;
 - 2: Initialize the target coordinates $\hat{\mathbf{z}}_0 = [0, 0]^T$;
 - 3: **for** $n = 1 : iter$ **do**
 - 4: Use formula (17) to get $\hat{\mathbf{z}}_m$;
 - 5: Calculate Ψ' based on formula (24);
 - 6: Perform the second WLS estimation to obtain $\hat{\mathbf{z}}_p$ based on formula (25) ;
 - 7: Update parameter estimate $\hat{\mathbf{z}}_n = \pm\sqrt{\hat{\mathbf{z}}_p}$;
 - 8: Compute covariance matrix \mathbf{Q} according to formula (29) to (30);
 - 9: **if** $\|\hat{\mathbf{z}}_n - \hat{\mathbf{z}}_{n-1}\| \leq \epsilon$ **then**
 - 10: Exit **for** loop
 - 11: **end if**
 - 12: **end for**
 - 13: $\tilde{\mathbf{p}} = \hat{\mathbf{z}}_n$
-

process of obtaining its covariance matrix. However, due to the independence of observed distance and anchor position errors, the distribution of the error vector becomes uncertain. As a result, we first assume the error vector covariance matrix is an n-dimensional identity matrix during the initial iteration process. Thus, the first weighted least squares (WLS) estimate of \mathbf{z} can be obtained as follows

$$\hat{\mathbf{z}}_m = (\mathbf{G}^T \mathbf{Q}^{-1} \mathbf{G})^{-1} \mathbf{G}^T \mathbf{Q}^{-1} \mathbf{h} \quad (17)$$

where $\mathbf{Q} = \mathbf{I}_N$ in the first iteration. Note that the value of $x^2 + y^2$ in \mathbf{z} is related to the coordinates of the target. By utilizing the initial estimated position $\hat{\mathbf{z}}_m$, along with the constraint conditions, a updated system of equations can be formulated for the second WLS estimation. The relationship between the first estimation and its true value is as follows

$$\begin{cases} \hat{\mathbf{z}}_m(1) = x + e_1 \\ \hat{\mathbf{z}}_m(2) = y + e_2 \\ \hat{\mathbf{z}}_m(3) = x^2 + y^2 + e_3 \end{cases} \quad (18)$$

while e_1, e_2 and e_3 denote estimated errors. By squaring both e_1 and e_2 , the system of equations (18) can be transformed into the following system

$$\begin{cases} 2xe_1 + e_1^2 = \hat{\mathbf{z}}_m^2(1) - x^2 \\ 2ye_2 + e_2^2 = \hat{\mathbf{z}}_m^2(2) - y^2 \\ e_3 = \hat{\mathbf{z}}_m(3) - (x^2 + y^2) \end{cases} \quad (19)$$

The left-hand side of this system represents the errors. The equations (19) can be simplified as

$$\psi' = \mathbf{h}' - \mathbf{G}'_m \mathbf{z}_p \quad (20)$$

where $\mathbf{h}' = \begin{bmatrix} \hat{z}_m^2(1) \\ \hat{z}_m^2(2) \\ \hat{z}_m^2(3) \end{bmatrix}$, $\mathbf{G}' = \begin{bmatrix} 1 & 0 \\ 0 & 1 \\ 1 & 1 \end{bmatrix}$ and $\mathbf{z}_p = \begin{bmatrix} x^2 \\ y^2 \end{bmatrix}$. $\boldsymbol{\psi}'$ is error vector of \mathbf{z}_p and can be transformed into

$$\begin{cases} \psi'_1 = 2xe_1 + e_1^2 \approx 2xe_1 \\ \psi'_2 = 2ye_2 + e_2^2 \approx 2ye_2 \\ \psi'_3 = e_3 \end{cases} \quad (21)$$

In order to determine the weights for the second WLS estimate, the covariance matrix of the first WLS estimate is required, and this can be achieved using the perturbation method [2], [28]. The perturbation of \mathbf{z}_m can be approximated as follows

$$\Delta \mathbf{z}_m \approx (\mathbf{G}^T \mathbf{Q}^{-1} \mathbf{G})^{-1} \mathbf{G}^T \mathbf{Q}^{-1} \delta \quad (22)$$

$$\text{cov}(\mathbf{z}_m) = \mathbb{E}[\Delta \mathbf{z}_m \Delta \mathbf{z}_m^T] = (\mathbf{G}^T \mathbf{Q}^{-1} \mathbf{G})^{-1} \quad (23)$$

Subsequently, the covariance matrix of $\boldsymbol{\psi}'$ is given by

$$\boldsymbol{\Psi}' = \mathbb{E}[\boldsymbol{\psi}' \boldsymbol{\psi}'^T] = 4\mathbf{B}' \text{cov}(\mathbf{z}_m) \mathbf{B}' \quad (24)$$

where $\mathbf{B}' = \text{diag}(x, y, 0.5)$. Consequently, the estimated value of \mathbf{z}_p can be expressed as

$$\hat{\mathbf{z}}_p = (\mathbf{G}'^T \boldsymbol{\Psi}'^{-1} \mathbf{G}')^{-1} \mathbf{G}'^T \boldsymbol{\Psi}'^{-1} \mathbf{h}' \quad (25)$$

Since \mathbf{B}' involves the true position of the target, it can be initially substituted with the estimated values $\hat{z}_m(1)$ and $\hat{z}_m(2)$ obtained from the first WLS solving process. By performing two consecutive WLS computations, the localization result of the target is obtained as follows

$$\hat{\mathbf{z}} = \pm \sqrt{\hat{\mathbf{z}}_p} \quad (26)$$

Next, we utilize $\hat{\mathbf{z}}$ to optimize the error covariance matrix for the first WLS. Based on formula (21) and $\delta_i \ll d_i$, we can derive the estimation error for the first WLS.

$$e_i = 2\|\mathbf{p} - \mathbf{s}_i\| \xi_i + \xi_i^2 \approx 2\|\mathbf{p} - \mathbf{s}_i\| \xi_i \quad (27)$$

where $\xi_i = d_i - \|\mathbf{p} - \mathbf{s}_i\|$. Thus, the squared error vector \mathbf{e} can be written as

$$\mathbf{e} = 2\mathbf{B}\boldsymbol{\xi} \quad (28)$$

Because $B = \text{diag}(\|\mathbf{p} - \mathbf{s}_i\|), i = 1, 2, \dots, N$ is the set of true distances between \mathbf{p} and \mathbf{s}_i , we substitute d_i in place of it. Therefore, the covariance matrix $\boldsymbol{\Psi}$ of the error vector \mathbf{e} can be given by

$$\boldsymbol{\Psi} = \mathbb{E}(\mathbf{e}\mathbf{e}^T) = 4\mathbf{B}\mathbb{E}(\delta\delta^T)\mathbf{B} = 4\mathbf{B}\mathbf{Q}\mathbf{B} \quad (29)$$

where $\boldsymbol{\xi} = [\xi_1, \xi_2, \dots, \xi_N]^T$ and \mathbf{Q} is the covariance matrix of the distance error vector. Considering the coordinates estimated as $\hat{\mathbf{z}}$ in the second WLS estimation, we can optimize \mathbf{Q} as follows

$$\mathbf{Q} = \text{diag}(\xi_1^2, \xi_2^2, \dots, \xi_N^2) \quad (30)$$

where

$$\xi_i = r_i - \|\hat{\mathbf{z}} - \mathbf{s}_i\|. \quad (31)$$

Utilizing the estimated coordinates in formula (26), we can optimize the covariance matrix of distance errors for the next iteration. In summary, each iteration consists of two steps: estimating coordinates using two consecutive WLS

computations and updating the covariance matrix of distance errors once. This process continues until either the maximum iteration count *iter* is reached or the estimated coordinates from two consecutive iterations satisfy the convergence criterion ϵ , indicating algorithm convergence. The iChan algorithm is concluded in Algorithm 1.

After obtaining the estimation $\tilde{\mathbf{p}}$ and knowing the approximate coordinates $\tilde{\mathbf{s}}_i$ of the dynamic anchors, we can set its neighborhood as the search domain to solve (15). In order to fully leverage the positional information and CRLB of neighboring nodes, we propose an advanced two-step TOA localization algorithm based on CRLBs. Define $B(\mathbf{s}, r)$ to represent a circular neighborhood with its center at coordinate point \mathbf{s} and a radius of r . Thus the MLE problem in (15) can be written as

$$\begin{aligned} \min_{\mathbf{p}^k, \mathbf{s}_i} \quad & \sum_{i=1}^N \frac{(r_i - \|\mathbf{p}^k - \mathbf{s}_i\|)^2}{\sigma^2} + \sum_{i=1}^N \frac{\|\tilde{\mathbf{s}}_i - \mathbf{s}_i\|^2}{\sigma_{ci}^2} \\ \text{s.t.} \quad & \mathbf{s}_i \in B(\tilde{\mathbf{s}}_i, r_s) \\ & \mathbf{p}^k \in B(\tilde{\mathbf{p}}^k, r_p) \end{aligned} \quad (32)$$

In Equation (32), it is noteworthy that while solving for \mathbf{p} , estimates of its neighboring dynamic anchors \mathbf{s}_i are simultaneously derived by utilizing lower-level neighbors. After employing the PSO algorithm, the updated dynamic anchors are denoted as $\tilde{\mathbf{s}}'_i$.

Remark 1. The updated estimation accuracy of dynamic anchors is higher than that of the initial estimation. Intuitively, $\tilde{\mathbf{s}}'_i$, on top of $\tilde{\mathbf{s}}_i$, integrates distance constraints for serving as dynamic anchors in localizing higher-level nodes. This integration is depicted by the first term in Equation (32), resulting in significantly improved performance. The validation of this enhancement finds support in the CRLB and can be further proven mathematically in Appendix B.

Given the superior precision of $\tilde{\mathbf{s}}'_i$ compared to $\tilde{\mathbf{s}}_i$, we employ $\tilde{\mathbf{s}}'_i$ as the estimated dynamic anchors for the secondary estimation of \mathbf{p} . The objective function is as follows

$$\begin{aligned} \min_{\mathbf{p}^k, \mathbf{s}_i} \quad & \sum_{i=1}^N \frac{(d_i - \|\mathbf{p}^k - \mathbf{s}_i\|)^2}{\sigma^2} + \sum_{i=1}^N \frac{\|\tilde{\mathbf{s}}'_i - \mathbf{s}_i\|^2}{(\sigma_{ci}')^2} \\ \text{s.t.} \quad & \mathbf{s}_i \in B(\tilde{\mathbf{s}}_i, r_s) \\ & \mathbf{p}^k \in B(\tilde{\mathbf{p}}^k, r_p) \end{aligned} \quad (33)$$

where the first term aligns with Equation (32). On the other hand, $(\sigma_{ci}')^2$ represents a modification of σ_{ci}^2 . This modification incorporates information from the target \mathbf{p}^k into the FIM, resulting in a reduced CRLB utilized for the subsequent estimation. Ultimately, this problem remains amenable to resolution using the PSO algorithm, facilitating the attainment of the final estimation outcome for the subsequent step.

C. Robust TOA Algorithm for Mobile Environments

In MANETs, node mobility stands as a formidable challenge for localization due to its profound impact on network topology and anchor point selection. Taking into account that each network node possesses memory and storage capabilities, we have enhanced the static algorithm's performance by

Algorithm 2 Two-step TOA Localization Algorithm Based on CRLB

Input:

- Initial dynamic anchor estimate $\tilde{\mathbf{s}}_i, i = 1, 2, \dots, N$;
- Initial CRLBs for dynamic anchors $\sigma_{ci}^2, i = 1, 2, \dots, N$;
- Observed distances d_i between \mathbf{s}_i and target \mathbf{p} ;

Output: The estimated coordinates of target nodes $\hat{\mathbf{p}}$;

- 1: Use iChan method in Algorithm 1 to obtain approximate estimation $\tilde{\mathbf{p}}$ for the target node \mathbf{p} ;
 - 2: Form search neighborhood $B(\tilde{\mathbf{s}}_i, r_s)$ and $B(\tilde{\mathbf{p}}, r_p)$;
 - 3: Solve problem in (32) using the PSO method to update the dynamic anchors $\tilde{\mathbf{s}}'_i, i = 1, 2, \dots, N$;
 - 4: Update CRLBs $(\sigma_{ci}^2)'$ for dynamic anchor errors by employing $\tilde{\mathbf{s}}'_i$;
 - 5: Solve problem in (33) using the PSO method to get the final estimation $\hat{\mathbf{p}}$;
-

incorporating the previous moment's location information into the existing algorithm, making our method more robust in MANETs.

Given the pronounced dynamics of the MANET, both base anchors and other blind nodes adhere to a mobility model that merges the Random Waypoint Mobility Model (RWM) and Random Direction (RD) model. This mobility model computes node movement speed as a vector summation of average and random speeds. Consequently, we represent the coordinates of a dynamic node within a MANET at a specific sampling time as follows

$$\begin{aligned} x_t &= x + v_2 \times \cos(\theta_2) \times \Delta t \\ &= x + (v_{\text{mean}} + v_n) \cos(R_\theta(t)) \Delta t \\ y_t &= y + v_2 \times \sin(\theta_2) \times \Delta t \\ &= y + (v_{\text{mean}} + v_n) \sin(R_\theta(t)) \Delta t \end{aligned} \quad (34)$$

where $\mathbf{p} = (x, y)^T$ and $\mathbf{p}_t = (x_t, y_t)^T$ are the initial and post-movement coordinates of dynamic nodes, respectively.

Consider a target node \mathbf{p} at sampling time t_1 , denoted as \mathbf{p}_{t1} , and at a subsequent time t_2 , denoted as \mathbf{p}_{t2} . Assuming $t_2 > t_1$, we can obtain the past-time estimation $\hat{\mathbf{p}}_{t1}$ at next time t_2 . Our dynamic approach aims to optimize the current computation through past-time position estimations. It's important to note that estimations of past-time node positions are reliant on anchor-based localization, and thus their accuracy remains uncertain. Furthermore, the motion model of the node involves intricate, random movement patterns. Therefore, it is not reasonable to impose strict and inflexible constraints directly in our dynamic method.

In this subsection, we introduce a penalty term as a soft constraint by penalizing excessive position changes between two sampling time. The penalty factor is adjusted to maintain the balance of the previous estimation rather than imposing hard constraints. Illustrated in Algorithm 2, the first step aims to refine anchor coordinates in our original two-step TOA algorithm, as outlined in the formula (32). This step remains unchanged in our dynamic algorithm. However, in the context of the second step, alongside optimizing anchor coordinates, our dynamic algorithm introduces mobility constraints. There-

fore, the optimization problem presented in the formula (33) can be reformulated as follows

$$\begin{aligned} \min_{\mathbf{p}_{t2}, \mathbf{s}_i} \quad & \sum_{i=1}^N \left(\frac{(r_i - d_i)^2}{\sigma^2} + \frac{\|\tilde{\mathbf{s}}'_i - \mathbf{s}_i\|^2}{(\sigma_{ci}^2)'} \right) + \eta (r_{t1t2} - d_m)^2 \\ & \mathbf{s}_i \in B(\tilde{\mathbf{s}}'_i, r_i) \\ & \mathbf{p}_{t2} \in B(\tilde{\mathbf{p}}_{t2}, r) \\ \text{s.t.} \quad & d_m = v_{\text{mean}} (t_2 - t_1) \\ & d_i = \|\mathbf{p}_{t2} - \mathbf{s}_i\| \\ & r_{t1t2} = \|\mathbf{p}_{t2} - \hat{\mathbf{p}}_{t1}\| \end{aligned} \quad (35)$$

where η is the penalty factor. When the time interval between t_2 and t_1 is sufficiently small, the motion of node \mathbf{p} can be approximated as linear, and accordingly, we establish the mobility constraint. Ultimately, the PSO algorithm can then be employed to address this problem and yield the conclusive estimation outcome for the second step. The refined two-step TOA localization algorithm tailored for mobile environments is succinctly outlined in Algorithm 3.

Algorithm 3 Two-step TOA localization algorithm for mobile environments

Input:

- Initial dynamic anchor estimate $\tilde{\mathbf{s}}_i, i = 1, 2, \dots, N$;
- Initial CRLBs for dynamic anchors $\sigma_{ci}^2, i = 1, 2, \dots, N$;
- Observed distances d_i between \mathbf{s}_i and target \mathbf{p}_{t2} ;
- Previous target estimate $\hat{\mathbf{p}}_{t1}$ at past time t_1 ;

Output: The current coordinates estimate of target nodes $\hat{\mathbf{p}}_{t2}$;

- 1: Use iChan method in Algorithm 1 to obtain approximate estimation result $\tilde{\mathbf{p}}_{t2}$ for the target node \mathbf{p} ;
 - 2: Form search neighborhood $B(\tilde{\mathbf{s}}_i, r_s)$ and $B(\tilde{\mathbf{p}}, r_p)$;
 - 3: Solve problem in (32) using PSO method to update the estimation result for dynamic anchors $\tilde{\mathbf{s}}'_i, i = 1, 2, \dots, N$;
 - 4: Update CRLBs $(\sigma_{ci}^2)'$ for dynamic anchor errors by employing $\tilde{\mathbf{s}}'_i$;
 - 5: Solve problem in (35) using the PSO method to get the final estimation $\hat{\mathbf{p}}_{t2}$;
-

V. NUMERICAL SIMULATIONS

In this section, we conduct numerical simulations to assess our proposed method's robustness within MANETs. Firstly, we estimate the coordinates of a non-direct node to validate the performance of our approach in simple scenarios. We employ the CRLB as the benchmark to assess the accuracy of our estimations. Following this, we simulate a scenario of a mobile ad hoc network, applying our node localization method to tackle the challenges posed by highly dynamic environments.

A. Evaluation of Two-step TOA Localization Algorithm Based on CRLB

In this subsection, we validate our designed TOA algorithm, assessing its localization accuracy for a single node while benchmarking it against other established algorithms. Our algorithm specifically caters to localization concerns in level-2 or above nodes. Thus, we set the communication radius

between nodes at 500 m, establishing the foundation for hierarchical localization. To simplify, we envision a scenario comprising nine nodes: four at level 0, four at level 1, and one at level 2. Assuming an initial presence of four base anchors, each characterized by Gaussian-distributed position errors, we randomly select the true coordinates \mathbf{s}_i^0 to be

$$(134, 103)^T, (155, 205)^T, (103, 220)^T, (35, 264)^T$$

However, we only know the coordinates of anchor nodes with additive Gaussian errors whose standard deviation (represented by $\delta\mathbf{I}_2$) is 3 m for each component. Furthermore, the initial positions of the level-1 nodes \mathbf{p}_i^1 are established as follows

$$(431, 232)^T, (324, 577)^T, (200, 398)^T, (498, 245)^T$$

Considering a level-2 node \mathbf{p}^2 as the target with an initial position of $(600, 450)^T$, the observed distances between each connected pair of nodes follow a Gaussian distribution with a variance of σ . In the first step of our method, we aim to obtain more accurate estimates of neighbor dynamic anchors. For example, $\mathbf{p}_1^1 = (431, 232)^T$ is a level-1 node, it can be estimated by level-0 nodes as well as serves as a dynamic anchor point to locate level-2 node \mathbf{p}^2 . We compute the Root Mean Squared Error (RMSE) for the positioning outcomes through multiple simulations, which is determined by the number of simulations N and can be expressed as

$$\text{RMSE} = \sqrt{\frac{1}{N} \sum_{i=1}^N ((\hat{x}_i - x)^2 + (\hat{y}_i - y)^2)} \quad (36)$$

In Fig. 2, the depiction showcases the position errors of node \mathbf{p}_1^1 based on two independent estimates affected by different distance errors. In the initial estimation, node \mathbf{p}_1^1 solely serves as a target point, utilizing level-0 nodes for localization, achieving accuracy aligned with the initial CRLB. On the other hand, if this node functions as a dynamic anchor for the level-2 node \mathbf{p}^2 , the resultant CRLB is lower than the initial one. For this reason, a subsequent estimation for this level-1 node is pursued. In accordance with the first step of our method, this supplementary estimation for the level-1 node approaches the updated CRLB accuracy. Examining the outcomes across varying distance errors in Fig. 2, when the distance measurement errors among the network nodes escalate, the second positional outcome for the level-1 node consistently outperforms its initial estimation results.

In Fig. 3, the accuracy of our proposed algorithm for locating a level-2 node is verified and the robustness of the algorithm is examined by setting diverse observed distance measurement errors. Consistently, we maintain a fixed standard deviation of 3 m for the base anchor position error. To our knowledge, since there are fewer algorithms that use TOA multilevel localization within MANET scenarios, our comparative analysis involves contrasting our algorithm with other direct TOA localization methods, particularly in scenarios where anchor points exhibit errors.

The simulation results demonstrate that our algorithm achieves remarkable proximity to the CRLB for localizing a level-2 node that cannot be directly located by base anchors

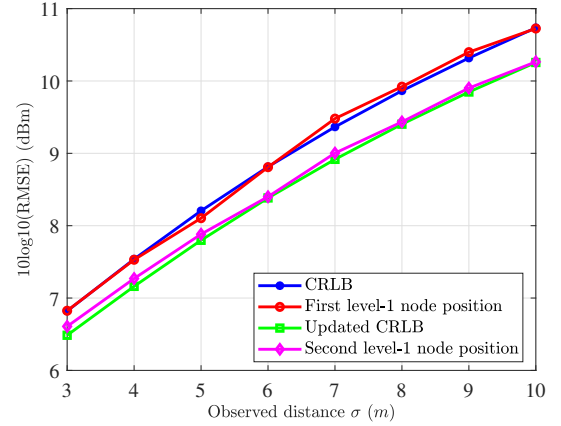


Fig. 2. Illustration of one level-1 node positioning error in different distance errors

when the distance error remains small. In Fig.3, our two-step TOA-CRLB localization algorithm, closely approaches the theoretical error limit when the standard deviation of observed distance errors measures 8 m or less. However, as the observed distance error continues to increase, our algorithm's performance starts to deteriorate gradually.

Comparatively, in contrast to conventional mathematical solutions represented by the SDP algorithm and optimization algorithms like PSO, neither category can attain the CRLB even in scenarios with minimal observed distance noise. Moreover, when confronted with substantial observed distance errors, both these algorithm types degrade rapidly. Notably, when the standard deviation of the distance error surpasses 5 m, degradation becomes more pronounced, reaching a critical point above 8 m. Conversely, our algorithm maintains a higher level of accuracy, exhibiting superior resilience under challenging conditions with large observed distance errors.

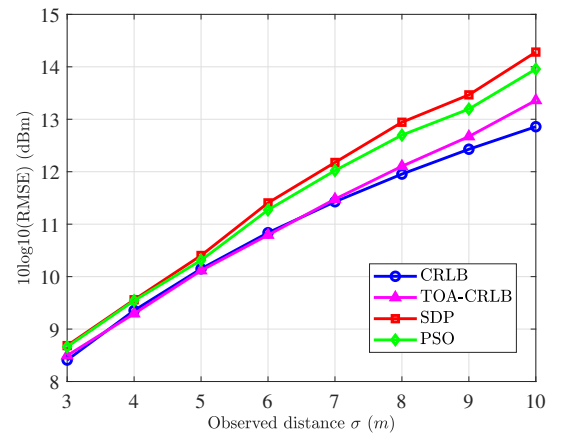


Fig. 3. Impact of the distance errors on the RMSE performance of level-2 node positioning

To assess the robustness of our dynamic algorithm in a mobile environment, we implement the mobility models described in the formula (34) across all nodes. The average velocity and time intervals are set at 10 m/s and 1 second, respectively. The standard deviations for base anchors and

observed distance errors are 3 m and 5 m, correspondingly. In Fig. 4, we evaluate the performance of the proposed algorithm 3 concerning the selection of penalty factor η . Additionally, we compare its performance with the initial algorithm outlined in Algorithm 2, alongside other existing TOA localization algorithms.

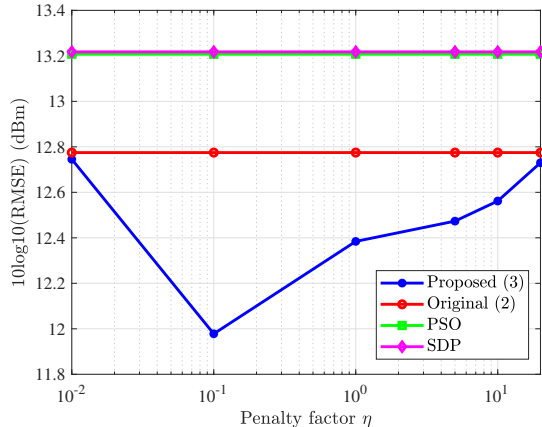


Fig. 4. RMSE performance of the proposed method in 3 under various penalty factors η

The penalty factor is set to vary from 10^{-2} to 20. From Fig. 4, it's evident that both the PSO and SDP algorithms maintain a considerable distance from our original static method in Algorithm 2, which is consistent with results in Fig. 2. Further simulations reveal that the RMSE of our dynamic method in Algorithm 3 stabilizes at the 12 dBm when penalty factor η is set to 10^{-1} . In comparison to our static method, it offers an improvement of around 0.8 dBm. Moreover, when contrasted with other algorithms, the accuracy gain is notably more substantial. Therefore, we opt to set the penalty factor to 10^{-1} for the subsequent validation processes.

B. 2D Localization System in a MANET Environment

For the practical realization of our designed TOA methodology, we create a multi-hop MANET scenario and perform simulations within a 2D localization system encompassing a square area of $1000m \times 1000m$, depicted in Fig. 5. The network consists of 50 nodes, where 4 nodes are designated as inaccurate base anchors at level 0, while the highest-tier nodes in the network are established as level-2 nodes. All network nodes exhibit dynamic behavior, maintaining an average movement speed from 10 m/s to 50 m/s.

Apart from the base nodes, functioning as level-0 nodes within the localization network, the hierarchical levels of other network nodes necessitate dynamic determination based on the quantity and levels of their neighboring nodes. These levels undergo real-time modifications within MANETs. Fig. 5 visually illustrates the evolving localization hierarchy across different time frames, showcasing dynamic fluctuations in the numbers of level-1 and level-2 nodes. Moreover, specific nodes adapt their levels and localization strategies in response to alterations in network topology. Due to the dynamic and complex nature of these environments, localizing the remaining nodes becomes more challenging.

C. Performance Evaluation of Level-2 Node Localization in MANETs

In this subsection, we showcase the practical application of our proposed algorithm for localizing level-2 nodes within MANETs, and compare with other wireless localization algorithms based on TOA measurements. The parameters of the simulation scene are given in Table II.

TABLE II. SIMULATION PARAMETERS

parameter	value	parameter	value
node number	50	base node number	4
transmission radius r	500m	average speed v_{mean}	10-50m/s
random speed v_n	0-5m/s	motion angle $R_\theta(t)$	$0-360i_c\alpha$
movement time T	20s	sampling interval Δt	0.2s
observed distance SD σ	3-10m	anchor position SD δ	3m

In our simulation scenario setup, the highest level for MANET nodes is 2, restricting direct connections with imprecise base anchors. Additionally, it is possible to expand node localization to higher levels beyond this limit. For level-1 nodes within MANETs, determining node positions still relies on error-prone anchor-based methods, considering the variability in available anchor locations and the varying numbers of neighboring base anchors. This approach mirrors the research presented in [23], [35]–[37]. Consequently, our algorithm primarily concentrates on resolving the localization challenges for nodes that are not directly located by level-0 nodes.

In the case of level-2 nodes, the number of these nodes varies over time, and any level-2 node can transition to a level-1 node due to random movement patterns. Therefore, analyzing the alterations of a single node is inadequate within practical scenario. Instead, it is imperative to compare the average RMSE of all level-2 nodes to validate the robustness of our algorithm, which is defined by $\epsilon_{\text{level2}} = \frac{1}{n_2} \sum_{i=1}^{n_2} \text{RMSE}(\mathbf{p}_i^2)$.

Fig. 6 illustrates the cumulative distribution function (CDF) of ϵ_{level2} across each sampling instance, with node average speed set at 20 m/s and observed distance standard deviation at 5 m. Our approach demonstrates remarkable accuracy in positioning estimation, with 90% of the average RMSE for all level-2 nodes held to within 10.2 m.

Furthermore, it demonstrates consistent positioning stability by maintaining an error margin of 3.71 m for all level-2 nodes. This greatly reduces the probability of target estimations with significant errors. Specifically, our median error reaches 8.85 m, which is in contrast to the median errors of 9.55 m, 9.71 m, 10.40 m, and 12.54 m observed in PSO [39], SDP [37], CWLLS [28] and LLS [27] methods, respectively. This superiority stems from its robustness against abrupt network topology changes and its adept utilization of reliable neighbor node positions.

In order to further verify the robustness of our method, we control the average speed of network nodes between 10 m/s and 50 m/s to ensure that the simulation results are consistent across a range of velocities. For the same sampling interval, besides the increased average movement speed, the standard deviation of observed distance errors σ has also increased from 3 m to 10 m. As illustrated in Fig. 7, our

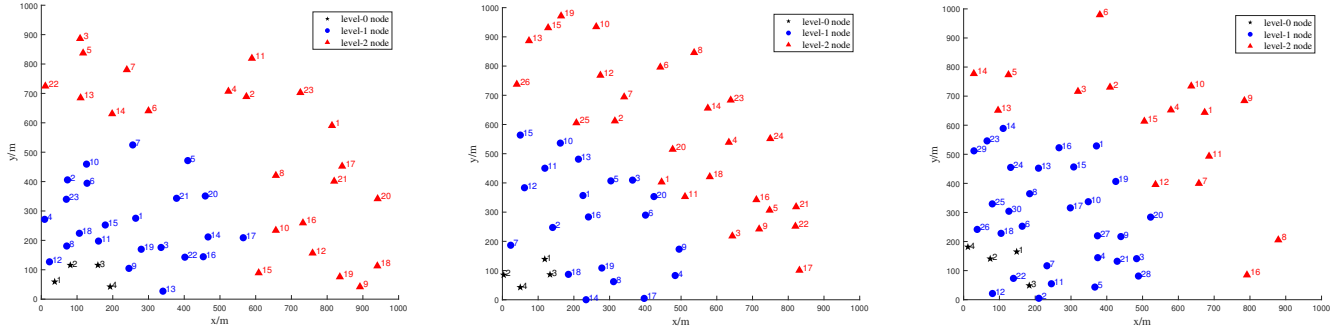


Fig. 5. Network node placement topology hierarchy at different time (a) movement time $T = 5s$; (b) movement time $T = 15s$; (c) movement time $T = 40s$.

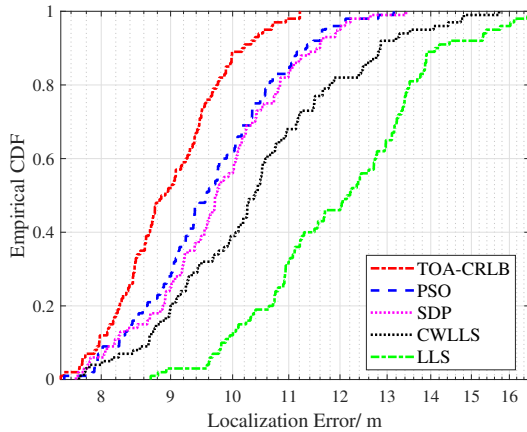


Fig. 6. CDF curve of average error in positioning level-2 nodes

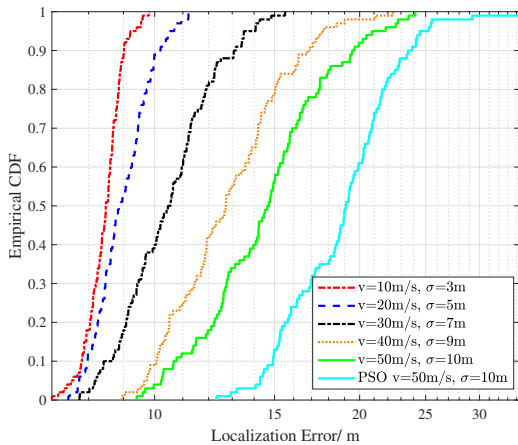


Fig. 7. Illustration of level-2 node positioning error under different velocities

method exhibits higher accuracy when the mobility speed and distance errors are low. When the mobility speed is below 20 m/s, our algorithm can achieve an accuracy of 10 m which meet the node positioning accuracy requirements for most networks under dynamic conditions [40]. Moreover, it maintains accuracy even when network node velocities undergo fluctuations. Even with a node average speed of 50

m/s, our algorithm still achieves a median error of 14.73 m for locating level-2 nodes. Notably, our method consistently yields smaller average errors compared to the utilization of the PSO algorithm, whose median error stands at 19.07 m. By using the CRLBs, the incorporation of two-step positioning outcomes not only enhances positioning accuracy but also mitigates the abrupt oscillations in dynamic anchor position errors resulting from the dynamic movements of nodes within the MANET.

VI. CONCLUSIONS

In this paper, we refine the TOA localization algorithm tailored for optimal deployment in MANETs. Firstly, we derive the CRLB as an evaluation benchmark and a guiding principle for our algorithm’s design, specifically catering to nodes position errors within a hierarchical MANET scenario. Secondly, we introduce a novel two-step TOA-CRLB localization approach to mitigate the error diffusion in cascaded localization. Leveraging CRLB insights and neighboring node positions, our method corrects neighbor node positions in the initial step to derive the final result. Extensive experimental results attest to the robustness and accuracy of our method, showcasing its superiority amidst substantial observed noise and complex dynamic settings compared to other TOA-based techniques. Future work will focus on integrating TOA with other localization algorithms to enhance the robustness of positioning accuracy in more challenging scenarios. Additionally, we aim to extend CRLB applications to enhance the precision of diverse wireless localization algorithms.

APPENDIX A DERIVATION OF THE FIM

We first define a concept where two nodes, s_i and s_j , satisfy the communication radius and possess different hierarchical levels. We term such nodes "cross-level nodes", where the lower-level node can serve as the dynamic anchor for the higher-level node. In cascading localization scenarios, we define $\theta = (\mathbf{p}^k, \mathbf{L}_{k-1}, \mathbf{L}_{k-2}, \dots, \mathbf{L}_0)$ as the estimator in the MLE framework. Based on this estimator, we derive the FIM

in our localization system. The log-likelihood function of the location estimation (ignoring the constant term) is given by

$$\begin{aligned} \mathbf{L}(\boldsymbol{\theta}) &\triangleq \sum_{i=1}^{d(\mathbf{p}^k)} f_1(d_i) + \sum_{i=1}^{\mathbf{n}_{k-1}} \sum_{j=1}^{d(\mathbf{s}_i)} f_2(d_{ij}) + \sum_{i=1}^{\mathbf{n}_0} f_3(\mathbf{s}_i^0) \\ f_1(d_i) &= -\frac{1}{2\sigma^2} (r_i - \|\mathbf{p}^k - \mathbf{s}_i\|)^2, \mathbf{s}_i \in D(\mathbf{p}^k) \\ f_2(d_{ij}) &= -\frac{1}{2\sigma^2} (r_{ij} - \|\mathbf{s}_i - \mathbf{s}_j\|)^2, \mathbf{s}_j \in D(\mathbf{s}_i) \\ f_3(\mathbf{s}_i^0) &= -\frac{1}{2\delta^2} \|\mathbf{s}_i^0 - \tilde{\mathbf{s}}_i^0\|^2, \mathbf{s}_i \in \mathbf{L}_0. \end{aligned} \quad (37)$$

where $d_i = \|\mathbf{p}^k - \mathbf{s}_i\|$ and $d_{ij} = \|\mathbf{s}_i - \mathbf{s}_j\|$. Substituting $\mathbb{E}(r_i) = d_i$, $\mathbb{E}(r_i^2) = d_i^2 + \sigma^2$ for $1 \leq m \leq 2$ and $1 \leq n \leq 2$, the (m, n) th element of the FIM is solely related to $f_1(d_i)$ in $\mathbf{L}(\boldsymbol{\theta})$ and is expressed as follows

$$\begin{aligned} [\mathcal{F}]_{m,n} &= -\mathbb{E} \left(\frac{\partial^2 \mathbf{L}(\boldsymbol{\theta})}{\partial \theta_m \partial \theta_n} \right) = -\sum_{i=1}^{d(\mathbf{p}^k)} \mathbb{E} \left(\frac{\partial^2 f_1(d_i)}{\partial d_i^2} \frac{\partial^2 d_i}{\partial p_m^k \partial p_n^k} \right) \\ &= \frac{1}{\sigma^2} \sum_{i=1}^{d(\mathbf{p}^k)} \frac{\partial^2 d_i}{\partial p_m^k \partial p_n^k} = \sum_{i=1}^{d(\mathbf{p}^k)} \frac{(p_m^k - s_{im})(p_n^k - s_{in})}{\sigma^2 \|\mathbf{p}^k - \mathbf{s}_i\|^2}. \end{aligned} \quad (38)$$

Additionally, we have, for $1 \leq m \leq 2 < n \leq 2(\mathbf{n}_{k-1} + 1)$, define $n = 2n_1 + n_2$, thus w_n in estimator $\boldsymbol{\theta}$ represents the n_2^{th} element of the n_1^{th} node of all nodes from the k -1 level and below, where $n_1 = 1, \dots, \mathbf{n}_{k-1}$ and $1 \leq n_2 \leq 2$. The (m, n) th element of the FIM is written as follows

$$\begin{aligned} [\mathcal{F}]_{m,n} &= -\mathbb{E} \left(\frac{\partial^2 \mathbf{L}(\boldsymbol{\theta})}{\partial \theta_m \partial \theta_n} \right) = -\mathbb{E} \left(\frac{\partial^2}{\partial d_{n_1}^2} f_1(d_{n_1}) \frac{\partial^2 d_{n_1}}{\partial p_m^k \partial p_{n_2}^k} \right) \\ &= \frac{1}{\sigma^2} \left(\frac{\partial^2 d_{n_1}}{\partial p_m^k \partial p_{n_2}^k} \right) = \frac{(p_m^k - s_{n_1 m})(p_{n_2}^k - s_{n_1 n_2})}{\sigma^2 \|\mathbf{p}^k - \mathbf{s}_{n_1}\|^2} \end{aligned} \quad (39)$$

where \mathbf{p}^k and \mathbf{s}_{n_1} are cross-level nodes. Similarly, for $3 \leq m \leq n \leq 2(\mathbf{n}_{k-1} + 1)$, define $m = 2m_1 + m_2$ represents the m_2^{th} element of the m_1^{th} node in estimator \mathbf{W} . The (m, n) th element of the FIM corresponding to $f_2(d_{ij})$ in $\mathbf{L}(\boldsymbol{\theta})$ is expressed as follows

$$\begin{aligned} [\mathcal{F}]_{m,n} &= -\mathbb{E} \left(\frac{\partial^2}{\partial d_{m_1 n_1}^2} f_2(d_{m_1 n_1}) \frac{\partial^2 d_{m_1 n_1}}{\partial s_{m_1 m_2} \partial s_{m_1 n_2}} \right) \quad (40) \\ &= \frac{1}{\sigma^2} \left(\frac{\partial^2 d_{m_1 n_1}}{\partial s_{m_1 m_2} \partial s_{m_1 n_2}} \right) = \frac{(s_{m_1 m_2} - s_{n_1 m_2})(s_{m_1 n_2} - s_{n_1 n_2})}{\sigma^2 \|\mathbf{s}_{m_1} - \mathbf{s}_{n_1}\|^2} \end{aligned}$$

where \mathbf{s}_{m_1} and \mathbf{s}_{n_1} are cross-level nodes. If $1 \leq m_1 = n_1 \leq (\mathbf{n}_{k-1} - \mathbf{n}_0)$, we have

$$\begin{aligned} [\mathcal{F}]_{m,n} &= -\sum_{i=1}^{d(\mathbf{s}_{m_1})} \mathbb{E} \left(\frac{\partial^2}{\partial d_{im_1}^2} f_2(d_{im_1}) \frac{\partial^2 d_{im_1}}{\partial s_{im_2} \partial s_{im_1 n_2}} \right) \\ &= \sum_{i=1}^{d(\mathbf{s}_{m_1})} \frac{(s_{m_1 m_2} - s_{im_2})(s_{m_1 n_2} - s_{in_2})}{\sigma^2 \|\mathbf{s}_{m_1} - \mathbf{s}_i\|^2} \end{aligned} \quad (41)$$

where \mathbf{s}_{m_1} is a node between level 1 and level $k-1$. Moreover, if $(\mathbf{n}_{k-1} - \mathbf{n}_0) \leq m_1 = n_1 \leq \mathbf{n}_{k-1}$ and $m_2 = n_2$ then point $\mathbf{s}_{m_1}^0$ is a base anchor, associated with both $f_2(d_{ij})$ and

$f_3(\mathbf{s}_i^0)$. The (m, n) th element of the FIM can be represented as follows

$$\begin{aligned} [\mathcal{F}]_{m,n} &= -\sum_{i=1}^{d(\mathbf{s}_{m_1})} \mathbb{E} \left(\frac{\partial^2 f_2(d_{im_1})}{\partial s_{im_2} \partial s_{im_1 n_2}} + \frac{\partial^2 f_3(\mathbf{s}_{m_1}^0)}{\partial^2 \mathbf{s}_{m_1 m_2}} \right) \\ &= \sum_{i=1}^{d(\mathbf{s}_{m_1})} \frac{(s_{m_1 m_2} - s_{im_2})^2}{\sigma^2 \|\mathbf{s}_{m_1} - \mathbf{s}_i\|^2} + \frac{\partial^2 \|\mathbf{s}_{m_1}^0 - \tilde{\mathbf{s}}_{m_1}^0\|^2}{2\delta^2 \partial^2 \mathbf{s}_{m_1 m_2}} \\ &= \sum_{i=1}^{d(\mathbf{s}_{m_1})} \frac{(s_{m_1 m_2} - s_{im_2})^2}{\sigma^2 \|\mathbf{s}_{m_1} - \mathbf{s}_i\|^2} + \frac{1}{\delta^2}. \end{aligned} \quad (42)$$

APPENDIX B PROOF OF REMARK 1

First, consider a target node \mathbf{p} alongside its dynamic anchors \mathbf{s}_i , where $i = 1, 2, \dots, n$. For the estimator $\boldsymbol{\theta} = (\mathbf{p}, \mathbf{s}_1, \mathbf{s}_2, \dots, \mathbf{s}_n)$, we compare the FIM in two separate estimations. When \mathbf{s}_i serves as the preceding-level target point, its covariance matrix is represented as $\boldsymbol{\Sigma}_{s_i}$, while the corresponding CRLB is indicated by σ_{ci}^2 . Initialize the covariance matrix of the target point as $\boldsymbol{\Sigma}_p$. Therefore, the FIM for the estimator $\boldsymbol{\theta}$ before localizing target \mathbf{p} is as follows

$$\mathcal{F}_{\text{in}} = \text{diag} [\boldsymbol{\Sigma}_p^{-1}, \boldsymbol{\Sigma}_{s_1}^{-1}, \boldsymbol{\Sigma}_{s_2}^{-1}, \dots, \boldsymbol{\Sigma}_{s_n}^{-1}]. \quad (43)$$

When \mathbf{s}_i serves as the dynamic anchor for target \mathbf{p} , the updated FIM is as follows

$$\mathcal{F}_{\text{up}} = -\mathbb{E} \left(\frac{\partial^2 \mathbf{L}(\boldsymbol{\theta})}{\partial \theta_m \partial \theta_n} \right) = \mathcal{F}_{\text{in}} + \mathbf{G}_d \quad (44)$$

where \mathbf{G}_d is the TOA-related sub-matrices. Based on the Section III, we have

$$\mathbf{G}_d = [\Delta \mathbf{p}, \Delta \mathbf{s}_1, \dots, \Delta \mathbf{s}_n]^T [\Delta \mathbf{p}, \Delta \mathbf{s}_1, \dots, \Delta \mathbf{s}_n] \quad (45)$$

where

$$\begin{aligned} \Delta \mathbf{p} &= \left[\sum_{i=1}^n \frac{\mathbf{p}_1 - \mathbf{s}_{i1}}{\sigma^2 \|\mathbf{p} - \mathbf{s}_i\|^2}, \sum_{i=1}^n \frac{\mathbf{p}_2 - \mathbf{s}_{i2}}{\sigma^2 \|\mathbf{p} - \mathbf{s}_i\|^2} \right], \\ \Delta \mathbf{s}_i &= \left[\frac{\mathbf{p}_1 - \mathbf{s}_{i1}}{\sigma^2 \|\mathbf{p} - \mathbf{s}_i\|^2}, \frac{\mathbf{p}_2 - \mathbf{s}_{i2}}{\sigma^2 \|\mathbf{p} - \mathbf{s}_i\|^2} \right], i = 1, \dots, n. \end{aligned} \quad (46)$$

Note that the matrix \mathbf{G}_d is positive definite. Consequently, we have

$$\mathcal{F}_{\text{up}} \succ \mathcal{F}_{\text{in}} \quad (47)$$

The CRLB is the diagonal elements in the inverse FIM. Therefore, the relationship between the CRLBs of the updated estimation and the initial one can be

$$(\sigma_{ci}^2)' < \sigma_{ci}^2 \quad (48)$$

Thus, we have proven that the accuracy of the updated dynamic anchors is higher than the previous ones.

REFERENCES

- [1] H. Zhang, S. Y. Tan, and C. K. Seow, "TOA-Based Indoor Localization and Tracking With Inaccurate Floor Plan Map via MRMSC-PHD Filter," *IEEE Sensors J.*, vol. 19, no. 21, pp. 9869–9882, 2019.
- [2] K. Yu, J. philippe Montillet, A. Rabbachin, P. Cheong, and I. Oppermann, "UWB location and tracking for wireless embedded networks," *Signal Process.*, vol. 86, no. 9, pp. 2153–2171, Sep. 2006.
- [3] Y.-Y. Li, G.-Q. Qi, and A.-D. Sheng, "Performance metric on the best achievable accuracy for hybrid toa/aoa target localization," *IEEE Commun. Lett.*, vol. 22, no. 7, pp. 1474–1477, 2018.
- [4] M. Tahboush and M. Agoyi, "A hybrid wormhole attack detection in mobile ad-hoc network (manet)," *IEEE Access*, vol. 9, pp. 11 872–11 883, 2021.
- [5] J. Huang, J. Liang, and S. Luo, "Method and Analysis of TOA-Based Localization in 5G Ultra-Dense Networks with Randomly Distributed Nodes," *IEEE Access*, vol. 7, pp. 174 986–175 002, Dec. 2019.
- [6] J. Dawes, "SDG interlinkage networks: Analysis, robustness, sensitivities, and hierarchies," *World Dev.*, vol. 149, p. 105693, Jan. 2022.
- [7] D. Niculescu and B. Nath, "DV based positioning in ad hoc networks," *Telecommun. Syst.*, vol. 22, pp. 267–280, Jan. 2003.
- [8] D. Jia, W. Li, P. Wang, X. Feng, H. Li, and Z. Jiao, "An advanced distributed mds-map localization algorithm with improved merging strategy," in *2016 IEEE International Conference on Information and Automation (ICIA)*. IEEE, 2016, pp. 1980–1985.
- [9] L. Gui, T. Val, A. Wei, and R. Dalce, "Improvement of range-free localization technology by a novel dv-hop protocol in wireless sensor networks," *Ad Hoc Networks*, vol. 24, pp. 55–73, 2015.
- [10] X. Chen, F. Dovis, S. Peng, and Y. Morton, "Comparative Studies of GPS Multipath Mitigation Methods Performance," *IEEE Trans. Aerosp. Electron. Syst.*, vol. 49, no. 3, pp. 1555–1568, Jul. 2013.
- [11] Y. Yuan, F. Shen, and X. Li, "GPS multipath and NLOS mitigation for relative positioning in urban environments," *Aerosp. Sci. Technol.*, vol. 107, p. 106315, Dec. 2020.
- [12] N. Fornaro, R. Giuliani, C. Noviello, D. Reale, and S. Verde, "Assimilation of GPS-Derived Atmospheric Propagation Delay in DInSAR Data Processing," *IEEE J. Sel. Topics Appl. Earth Observ. Remote Sens.*, vol. 8, no. 2, pp. 784–799, Feb. 2015.
- [13] H. Guo and P. Crossley, "Design of a Time Synchronization System Based on GPS and IEEE 1588 for Transmission Substations," *IEEE Trans. Power Del.*, vol. 32, no. 4, pp. 2091–2100, Aug. 2017.
- [14] M. Vossiek, L. Wiebking, P. Gulden, J. Wiegardt, C. Hoffmann, and P. Heide, "Wireless local positioning," *IEEE Microw. Mag.*, vol. 4, no. 4, pp. 77–86, Dec. 2003.
- [15] V. Savic, J. Ferrer-Coll, P. Angskog, J. Chilo, P. Stenumgaard, and E. G. Larsson, "Measurement Analysis and Channel Modeling for TOA-Based Ranging in Tunnels," *IEEE Trans. Wireless Commun.*, vol. 14, no. 1, pp. 456–467, Jan. 2015.
- [16] T. Pavlenko, M. Schutz, M. Vossiek, T. Walter, and S. Montenegro, "Wireless Local Positioning System for Controlled UAV Landing in GNSS-Denied Environment," in *Proc. IEEE 5th Int. Workshop Metro. Aerosp. (MetroAeroSpace)*, Jun. 2019, pp. 171–175.
- [17] N. Mansoor, M. I. Hossain, A. Rozario, M. Zareei, and A. R. Arreola, "A fresh look at routing protocols in unmanned aerial vehicular networks: A survey," *IEEE Access*, vol. 11, pp. 66 289–66 308, 2023.
- [18] F. B. Sorbelli, C. M. Pinotti, S. Silvestri, and S. K. Das, "Measurement Errors in Range-Based Localization Algorithms for UAVs: Analysis and Experimentation," *IEEE Trans. Mobile Comput.*, vol. 21, no. 4, pp. 1291–1304, Sep. 2020.
- [19] J. Shen, A. F. Molisch, and J. Salmi, "Accurate Passive Location Estimation Using TOA Measurements," *IEEE Trans. Wireless Commun.*, vol. 11, no. 6, pp. 2182–2192, Jun. 2012.
- [20] R. Kaune, J. Hájek, and W. Koch, "Accuracy analysis for toa localization in sensor networks," in *14th International Conference on Information Fusion*, 2011, pp. 1–8.
- [21] R. Peng and M. L. Sichitiu, "Angle of Arrival Localization for Wireless Sensor Networks," in *Proc. IEEE SECON*, vol. 1, Sep. 2006, pp. 374–382.
- [22] M. Jais, P. Ekan, R. Ahmad, I. Ismail, T. Sabapathy, and M. Jusoh, "Review of angle of arrival (AOA) estimations through received signal strength indication (RSSI) for wireless sensors network (WSN)," in *Proc. Int. Conf. Comput., Commun., Control Technol. (I4CT)*, Apr. 2015, pp. 354–359.
- [23] S. Zhao, X.-P. Zhang, X. Cui, and M. Lu, "A New TOA Localization and Synchronization System With Virtually Synchronized Periodic Asymmetric Ranging Network," *IEEE Internet Things J.*, vol. 8, no. 11, pp. 9030–9044, Jun. 2021.
- [24] Y. Zou and H. Liu, "Semidefinite Programming Methods for Alleviating Clock Synchronization Bias and Sensor Position Errors in TDOA Localization," *IEEE Signal Process. Lett.*, vol. 27, pp. 241–245, Jan. 2020.
- [25] R. Kaune, "Accuracy studies for TDOA and TOA localization," in *Proc. 15th Int. Conf. Inf. Fusion*, Jul. 2012, pp. 408–415.
- [26] N.-T. Nguyen and B.-H. Liu, "The mobile sensor deployment problem and the target coverage problem in mobile wireless sensor networks are np-hard," *IEEE Systems Journal*, vol. 13, no. 2, pp. 1312–1315, 2019.
- [27] Y. Wang, F. Zheng, M. Wiemeler, W. Xiong, and T. Kaiser, "Reference Selection for Hybrid TOA/RSS Linear Least Squares Localization," in *Proc. IEEE Veh. Technol. Conf. (VTC Fall)*, Sep. 2013, pp. 1–5.
- [28] Y. Kang, Q. Wang, J. Wang, and R. Chen, "A High-Accuracy TOA-Based Localization Method Without Time Synchronization in a Three-Dimensional Space," *IEEE Trans. Ind. Informat.*, vol. 15, no. 1, pp. 173–182, Jan. 2019.
- [29] W. Ding, S. Chang, X. Yang, S.-D. Bao, and M. Chen, "Genetic Algorithm with Opposition-based Learning and Redirection for Secure Localization Using ToA Measurements in Wireless Networks," *IEEE Internet Things J.*, pp. 1–1, Aug. 2023.
- [30] X. Zhu, Y. Zhang, and Q. Zhang, "An Improved DV-Hop Node Localization Algorithm Based on Sparrow Search for WSNs," in *Proc. IEEE 12th Int. Conf. Electron. Inf. Emergency Commun. (ICEIEC)*, Jul. 2022, pp. 154–157.
- [31] X. Lv, K. Liu, and P. Hu, "Geometry influence on gdop in toa and aoa positioning systems," in *2010 Second International Conference on Networks Security, Wireless Communications and Trusted Computing*, vol. 2, 2010, pp. 58–61.
- [32] D. Bajovic, B. Sinopoli, and J. Xavier, "Sensor Selection for Event Detection in Wireless Sensor Networks," *IEEE Trans. Signal Process.*, vol. 59, no. 10, pp. 4938–4953, Oct. 2011.
- [33] E. Kuiper and S. Nadjm-Tehrani, "Geographical Routing With Location Service in Intermittently Connected MANETs," *IEEE Trans. Veh. Technol.*, vol. 60, no. 2, pp. 592–604, Feb. 2011.
- [34] T. Jia and R. M. Buehrer, "A new Cramer-Rao lower bound for TOA-based localization," in *Proc. - IEEE Mil. Commun. Conf. MILCOM*, Nov. 2008, pp. 1–5.
- [35] Y. Zou and Q. Wan, "Asynchronous Time-of-Arrival-Based Source Localization With Sensor Position Uncertainties," *IEEE Commun. Lett.*, vol. 20, no. 9, pp. 1860–1863, Sep. 2016.
- [36] G. Yang, Y. Yan, H. Wang, and X. Shen, "Improved robust TOA-based source localization with individual constraint of sensor location," *Signal Process.*, vol. 196, p. 108504, Art. 2022.
- [37] Z. W. Mekonnen and A. Wittneben, "Robust TOA based localization for wireless sensor networks with anchor position uncertainties," in *Proc. IEEE Int. Symp. Pers., Indoor, Mobile Radio Commun. (PIMRC)*, Sep. 2014, pp. 2029–2033.
- [38] X. Shi, J. Su, Z. Ye, F. Chen, P. Zhang, and F. Lang, "A Wireless Sensor Network Node Location Method Based on Salp Swarm Algorithm," in *Proc. 2019 10th IEEE IDAACS*, vol. 1, Sep. 2019, pp. 357–361.
- [39] Y. Yang, X. Wang, D. Li, D. Chen, and Q. Zhang, "An Improved Indoor 3-D Ultrawideband Positioning Method by Particle Swarm Optimization Algorithm," *IEEE Trans. Instrum. Meas.*, vol. 71, pp. 1–11, Aug. 2022.
- [40] Z. Xiao and Y. Zeng, "An overview on integrated localization and communication towards 6G," *Sci. China Inf. Sci.*, vol. 65, pp. 1–46, Mar. 2022.
- [41] Y. Zheng, J. Liu, M. Sheng, and C. Zhou, "Exploiting fingerprint correlation for fingerprint-based indoor localization: A deep learning-based approach," in *Machine Learning for Indoor Localization and Navigation*. Springer, 2023, pp. 201–237.
- [42] M. Sheng, J. Li, and Y. Shi, "Routing protocol with QoS guarantees for ad-hoc network," *Electronics Letters*, vol. 39, no. 1, pp. 143–145, 2003.
- [43] D. Zhai, M. Sheng, X. Wang, Y. Li, J. Song, and J. Li, "Rate and energy maximization in SCMA networks with wireless information and power transfer," *IEEE Communications Letters*, vol. 20, no. 2, pp. 360–363, 2015.
- [44] J. Li, Z. J. Haas, and M. Sheng, "Capacity evaluation of multi-channel multi-hop ad hoc networks," in *2002 IEEE International Conference on Personal Wireless Communications*. IEEE, 2002, pp. 211–214.
- [45] D. Zhou, M. Sheng, J. Li, and Z. Han, "Aerospace Integrated Networks Innovation for Empowering 6G: A Survey and Future Challenges," *IEEE Communications Surveys & Tutorials*, 2023.

Replace this box by an image with a width of 1 in and a height of 1.25 in!

Your Name All about you and the what your interests are.

Coauthor Same again for the co-author, but without photo